# BL Lacertae: a study of quasi-stationary feature trajectories in the inner part of a relativistic jet

L.A. Hambardzumyan *[1,2], T.G. Arshakian †[1], and A.B. Pushkarev ‡[3]

[1]Byurakan Astrophysical Observatory after V.A. Ambartsumian, Armenia
[2]Astrophysical Research Laboratory, YSU, Armenia
[3]Crimean Astrophysical Observatory, Nauchny, Crimea

**Abstract**

Radio interferometric VLBA observations allow the mapping of relativistic jets with sub-milliarcsecond resolution, which enables the studying of the fine structure and dynamics of the jets in active galactic nuclei. A quasi-stationary component (QSC) near the radio core is observed in a number of blazars. VLBA monitoring of the BL Lacertae object at 15 GHz has shown that the QSC located at about 0.26 mas from the radio core is followed by superluminal components, whose dynamics forms the structure of the jet on parsec scales. We study the trajectory of the QSC using the 164 epochs taken from the MOJAVE (Monitoring Of Jets in Active galactic nuclei with VLBA Experiments) database. The trajectory of the QSC is complex, and we use a moving average smoothing filter to track the intrinsic motion of the QSC. At small time scales of few months, we find that the QSC makes a swinging motion with about 23 reversals over 20 years with an average period of about 0.5 years. The trajectories between the reversals have varying lengths with a mean value of about 30 $\mu$as ($\sim$ 0.04 pc) and curvatures of varying degrees. Number of clockwise reversals are about twice less than that of anticlockwise reversals.

***Keywords:*** *BL Lacertae objects: individual: BL Lacertae, galaxies: active, radio continuum: galaxies, galaxies: jets.*

## 1. Introduction

About 10% of active galactic nuclei (AGN) are radio-loud. The central engine transforms the accretion power of a disk orbiting around a supermassive black hole into the kinetic energy of relativistic plasma in bipolar outflows. Synchrotron radio emission is generated towards the observer by the jet plasma moving along the helical magnetic fields. Observations with interferometric radio telescopes make it possible to map the radio jets with the highest resolution. This opens a possibility to study the structure of the jet and its dynamics on sub-milliarcsecond scales.

As a class of radio-loud AGNs, blazars are characterised by jets oriented at small angles to the line of sight. In this article we study the archetypical source of this class, BL Lacertae, located at redshift $z = 0.0686$ (Vermeulen et al., 1995) (scale factor is 1.3 pc mas$^{-1}$). Monitoring of BL Lacertae with Very Long Baseline Array (VLBA) at 15 GHz has revealed that the jet consists of a bright radio core followed by a quasi-stationary component (QSC) at a distance of 0.26 mas. The latter is labeled as C7 (Arshakian et al., 2020, Cohen et al., 2014, 2015). Moving superluminal components appear to emerge beyond C7 component. Cohen et al. (2015) suggested that the dynamics of the quasi-stationary component C7 shapes the behavior of the jet downstream up to distances of hundreds parsecs. Arshakian et al. (2020) used larger data sample collected from 116 epochs (1999–2016) and confirmed the link between the large amplitudes of C7 shaking and excitation of superluminal transverse waves propagating downstream during both the active and stable states of the jet. They showed that C7 moves mostly with superluminal speeds ($\sim 2c$) and its on-sky brightness distribution is asymmetric along and across the jet axis.

Here, we use the VLBA monitoring data at 15 GHz accumulated during almost over 20 years time period (164 epochs), which is a part of the MOJAVE (Monitoring Of Jets in Active galactic nuclei with VLBA

*hambardzumyanlian@gmail.com, Corresponding author
†t.arshakian@gmail.com
‡pushkarev.alexander@gmail.com


doi: https://doi.org/10.52526/25792776-23.70.1-94

Experiments) program (Kellermann et al., 1998, Lister et al., 2018), to perform a detailed analysis of the C7 trajectory on sub-parsec scales.

## 2. Scatter of C7 positions

Data reduction, modeling and error estimation are described in Lister et al. (2009), Cohen et al. (2014, 2015) and Arshakian et al. (2020). The distribution of scattered positions of C7 for a time period of 1999.37–2019.97 is shown in Figure 1. The median center is at position $\mathrm{RA_{med}} = -0.051$ mas and $\mathrm{Dec_{med}} = -0.255$ mas. The line connecting the radio core and the median center of C7 is considered to be the central axis of the jet, which has a positional angle $\mathrm{PA} = -169°$. The scatter of C7 positions has a quasi-circular distribution ($\sim 0.1$ mas) with a slight elongation along the jet axis. To study the C7 motion, Arshakian

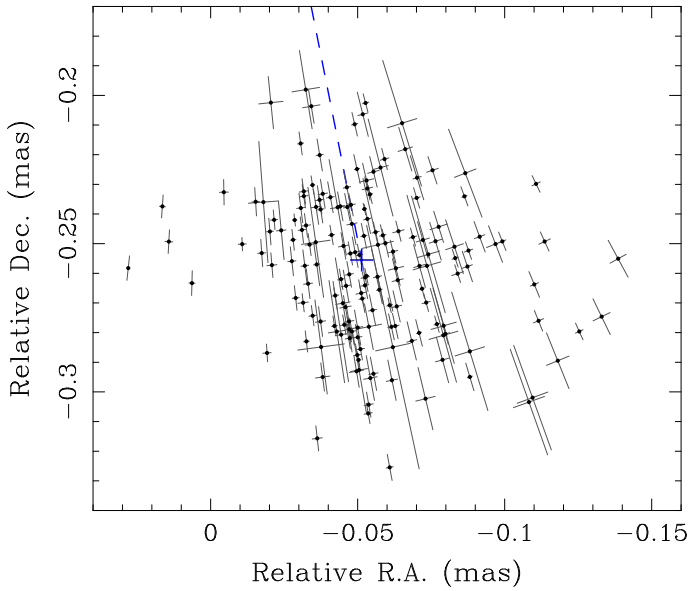


Figure 1. On-sky distribution of 164 positions of C7 in the RA–Dec plane. The positional errors of C7 are asymmetric along and across the jet. The jet central axis (dashed line) connects the radio core put at the phase center (0,0) with the median position of C7 (plus sign).

et al. (2020) introduced a displacement vector $\mathbf{r}$, which describes the direction of motion of C7 between two consecutive epochs. The time intervals $\Delta t$ between observations vary from a few days to several months with a median value of about 34 days. The median positional uncertainties of C7 along and across the jet are 5 $\mu$as and 2 $\mu$as, respectively. Arshakian et al. (2020) treated them as lower limits, while the real errors can be larger by a factor from 1.5 to 2.

## 3. Detailed analysis of trajectory of quasi-stationary component

We study the trajectory of C7 and its morphology for 164 epochs of observations, which is larger than that of Arshakian et al. (2020) by 48 epochs covering additional four years. The observed motion of C7 component is a combination of its intrinsic and asymmetric motion of the radio core, which occurs along the jet axis (Arshakian et al., 2020). It was estimated that the anisotropic core shift has a standard deviation 0.025 mas, while the C7 intrinsic motion has a mean displacement 0.02 mas and standard deviation 0.012 mas, implying that their contribution to the apparent motion of C7 are of comparable importance. To reduce the impact of the core shift we apply the moving average smoothing filter to apparent trajectory of C7 and thus recover the C7 intrinsic trajectory. In Figure 2, we present the C7 trajectory smoothed with sliding window of size $m = 4$ (where $m$ is the number of consecutive positions), which seems to be optimal for our study. In this case, the smoothing scale is about 0.055 mas, which translates to about 0.07 pc.

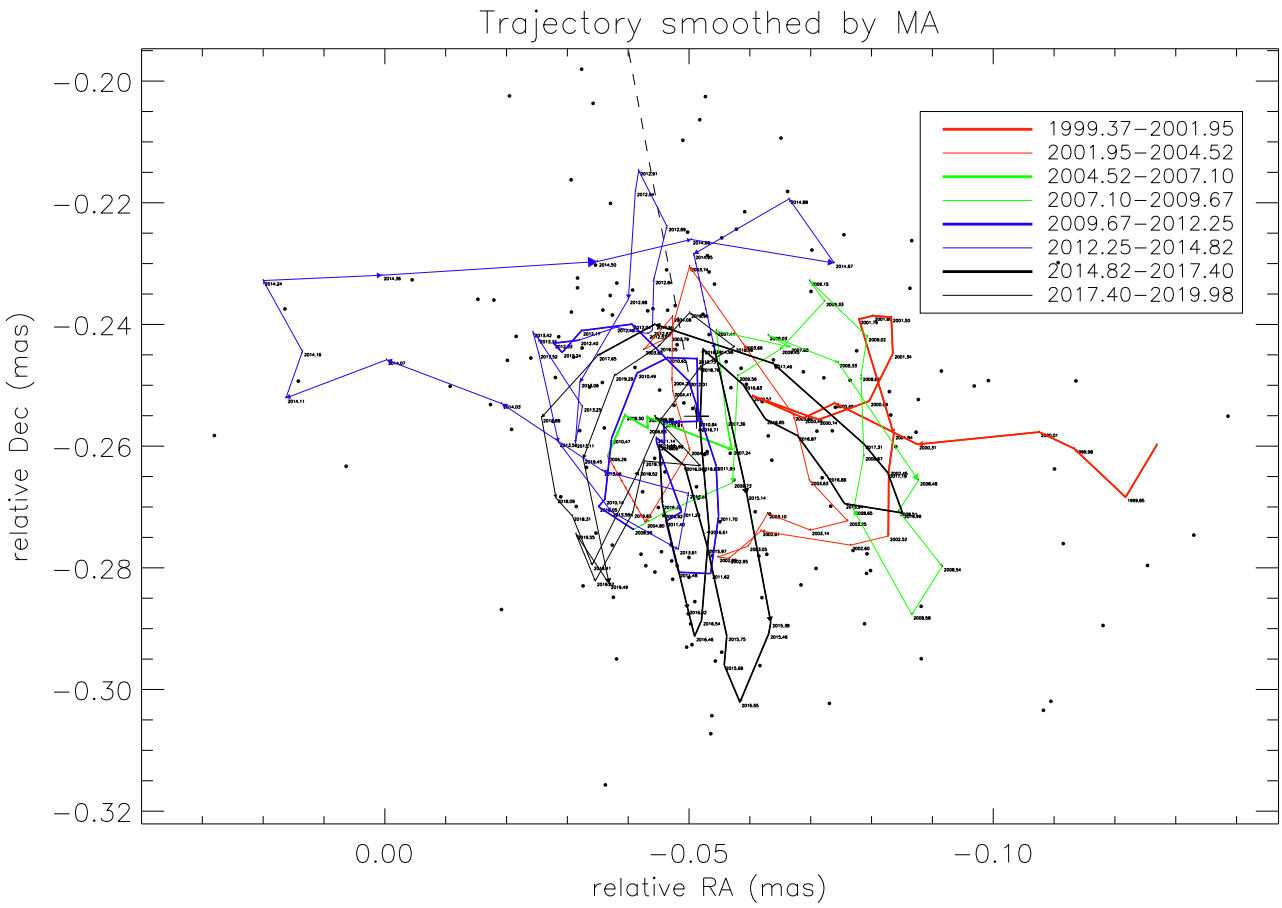


Figure 2. The apparent trajectory of C7 smoothed by moving average method with sliding window of length $m = 4$. The numbers along the smoothed trajectory are the observation epochs in years. The observed positions of C7 component are marked by dots. The radio core is at $(0, 0)$ position, which is connected with the median position of C7 (plus sign) by the jet central axis (dashed line). Thick and thin colored lines represent the time intervals of 2.95 years. Arrows indicate the direction of movement.

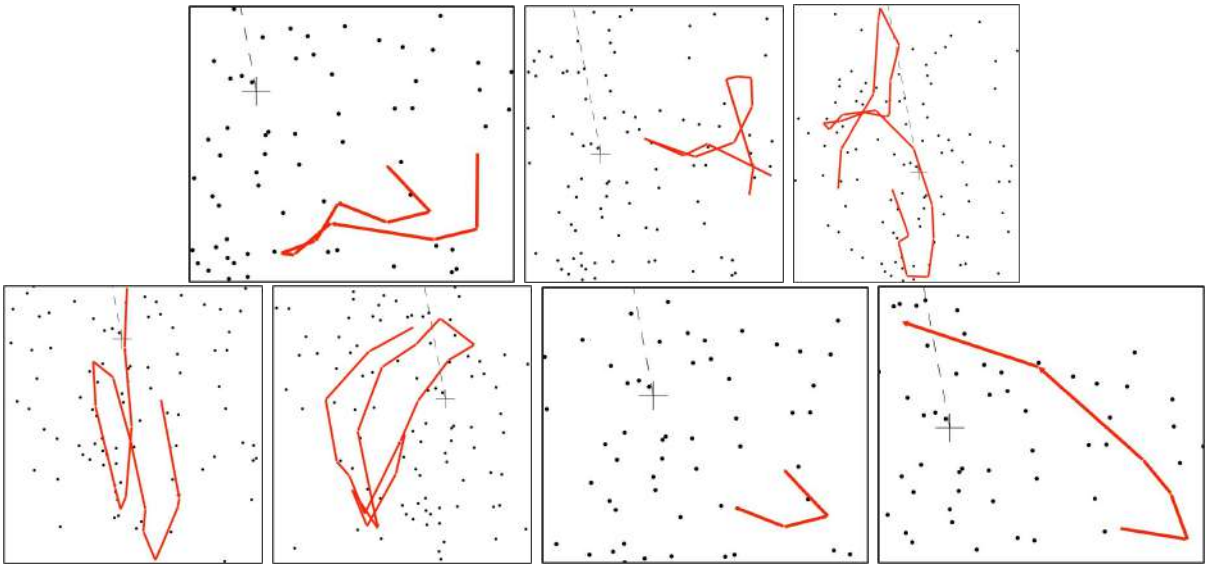

Figure 3. Examples of types of reversals: U-type irregular reversals (upper three panels), U-type quasi-regular reversals (lower first two panels), V-type reversal (third panel), and arch-like motion. The reversals shown occur during the following time intervals: 1 - 2001.79–2003.14, 2 - 2000.01–2001.84, 3 - 2011.00–2012.98, 4 - 2017.30–2019.63, 5 - 2014.95–2016.61, 6 - 2ßß2.96–2003.25, 7 - 2016.87–2017.31. The median position of the scatter is marked by a plus sign and dashed line connects the median position of C7 and radio core.


doi: https://doi.org/10.52526/25792776-23.70.1-94

Visual inspection of the trajectory reveals repetitive patterns, which may appear from a few to many times. Patterns like a reversing motion appear very frequently, there are also arch- and loop-like motion but they are less frequent. Between these patterns, the motion of C7 is represented by curving trajectories of varying degrees as well as quasi-oscillatory movements (see Figure 3).

Reversal motions on large spatial scales are conspicuous, e.g. component C7 moving westward and then reversing eastward during 2014–2014.5 (thin blue line in Figure 2) or component moving southward and reversing northward in 2015.55 during 2014.96-2016.04 (thick black line). Both reversals occur at spatial scales around 0.05 mas (0.07 pc) and have clockwise motion. It should be noted that most reversals occur on time scales of a few months.

### 3.1. Reversals and their characteristics

To define and characterise a reversal motion of C7 we introduce some criteria. We consider that a reversal is real if it consists of at least three successive segments of trajectory (or four epochs), which includes the reversal point and the angle at the reversal point is $< 90°$. We identify 23 reversals and among these we distinguish the U-turns ($< 45°$), V-turns ($> 45°$ and $< 90°$) and loop-like reversals (see Figure 3).

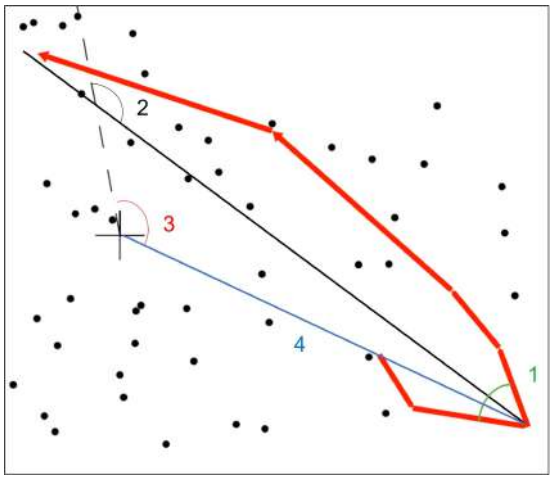


Figure 4. Characteristics of reversals: 1 - reversal angle, 2 - angle between jet and reversal direction, 3 - azimuthal angle, 4 - radial distance. Demonstrated is a typical U-reversal during 2016.85–2017.31. The median position of the scattered positions is marked by a plus sign and dashed line connects the median position of C7 and radio core.

To characterise the reversals, we performed the following measurements (see Figure 4):

- Reversal angle is the angle between two segments at the turning point. It is noticeable that 20 reversals have U-turns, 3 V-turns and among these 3 reversals have a loop-like structure.
- Time intervals between two successive reversals. Typical reversal period is about 0.5 yr and it is mostly ranged from 0.2 to 1.5 yr, with two outliers of about 3–3.5 yr (see Figure 5).
- Clockwise and counterclockwise direction of motion is defined at the turning point of a reversal. There are 15 counterclockwise and 8 clockwise reversals.
- Amplitude of reversals is the half of the length of segments making up the turn. The distribution of amplitudes has a mean value 0.032 mas and standard deviation 0.013 mas (Figure 6, top left panel). Amplitudes with the clockwise and counterclockwise reversals have similar distributions.
- Azimuthal angle is the angle between the median center and the turning point. Azimuthal angles of the clockwise and counterclockwise reversals have a uniform distribution. This tendency is true for the V-type reversals (Figure 6, bottom left panel).
- Radial distance is defined as the distance between the median center of scattered positions and the turning point. In Figure 6 (top right panel) it is clearly seen that the distribution of reversals are not random, there is a clustering of reversals at 0.029 mas with standard deviation 0.015 mas. Radial


doi: https://doi.org/10.52526/25792776-23.70.1-94

distances of the clockwise reversals (except one outlier) are smaller and lie within $\sim 0.03$ mas from the median center.

- Angle between the jet and the reversal direction. Angles for counterclockwise reversals have peak between 0° and 20° (Figure 6, bottom right panel), which indicates that majority of directions of counterclockwise reversals coincide with direction of the jet within 20°. Contrary, the angles of clockwise reversals have a uniform distribution.

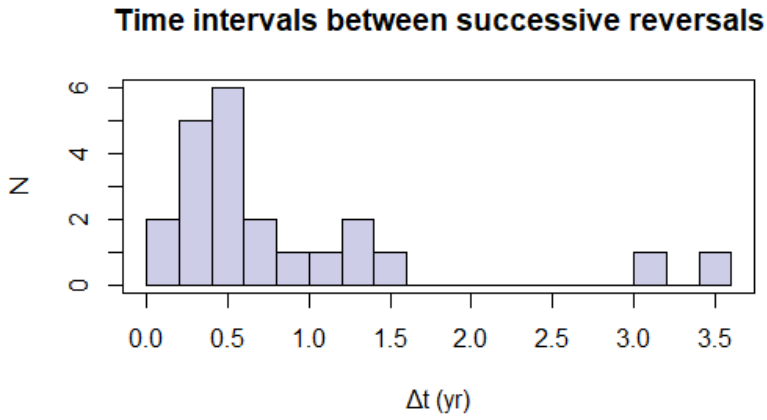


Figure 5. Distribution of time intervals between successive reversals.

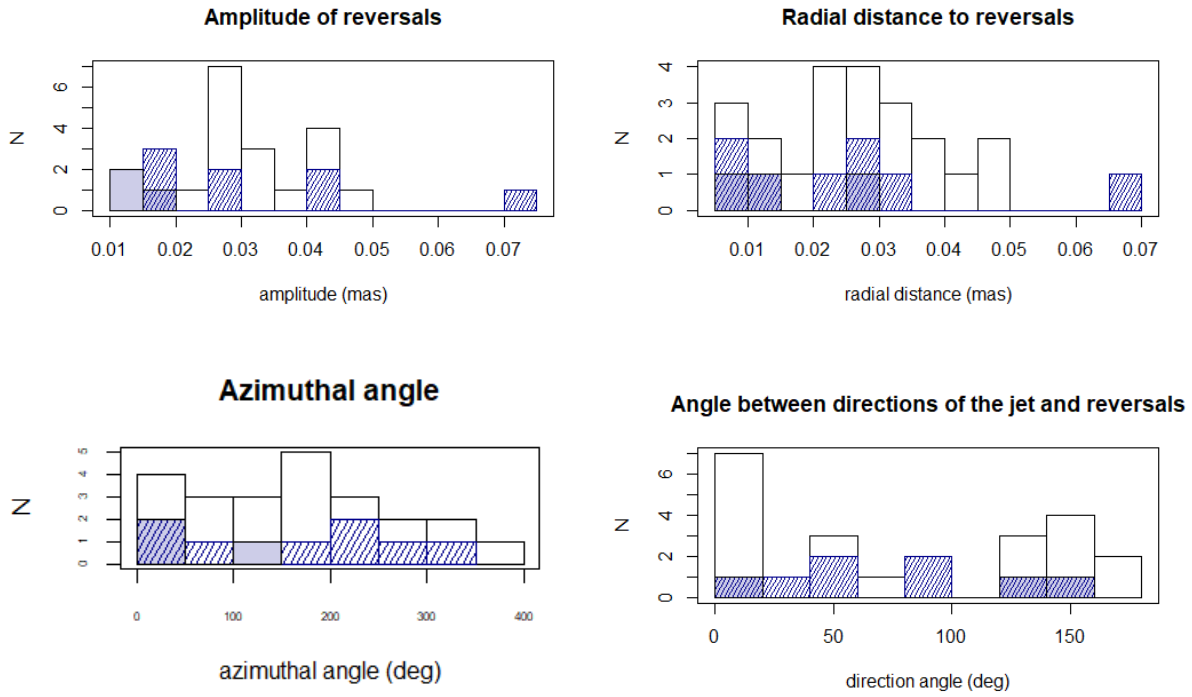


Figure 6. Distributions of amplitudes of reversals, radial distance to reversing point, azimuthal angle and angle between the jet and the direction of reversal. The white colour represents all types of reversals, the blue colour indicates the V-turns and the sloping blue lines indicate the clockwise reversals.

.

## 4. Discussion and Summary

A detailed analysis of the smoothed trajectory of the quasi-stationary C7 component shows that it performs swinging motion at various scales within 0.1 mas over a time period of 20 years. We identify


doi: https://doi.org/10.52526/25792776-23.70.1-94

recurrent motion patterns such as 20 U-type and 3 V-type reversals. The reversals occur with a typical period of 0.5 yr and the mean amplitude of about 0.03 mas. The fact that the component moves in most cases along a U-turn trajectory indicates the physical nature of this movement. Such motions can occur, for example, when a transverse wave passes along the jet, while the stationary component behaves like a seagull on a wave, i.e. moving across the stream. For BL Lac, the jet viewing angle is about 8° (Cohen et al., 2015), so the component will make reversal movements from the observer's point of view. In this case, changing the angle between the jet and reversal direction (Figure 4) means generating a new transverse wave in the jet. It is known that transverse waves move with relativistic velocities of the order of 0.95–0.98 of the speed of light (Cohen et al., 2015), which can form an illusion of superluminal velocities of the quasi-stationary component in the observer's rest of frame. The measurement of superluminal velocities of C7 component exceeding the speed of light by two times was found by Arshakian et al. (2020). A detailed study of such a scenario will be carried out in subsequent papers.

The number of the counterclockwise turns is more than twice the number of clockwise turns. To understand such a significant difference, it is necessary to investigate at what time and spatial scales the reversals occur. The same applies to the angle between the jet and reverse directions.

**Acknowledgements**

The VLBA is a facility of the National Radio Astronomy Observatory, a facility of the National Science Foundation that is operated under cooperative agreement with Associated Universities, Inc. This research has made use of data from the MOJAVE database that is maintained by the MOJAVE team (Lister et al., 2018).

## References

Arshakian T. G., Pushkarev A. B., Lister M. L., Savolainen T., 2020, Astron. Astrophys. , 640, A62

Cohen M. H., et al., 2014, Astrophys. J. , 787, 151

Cohen M. H., et al., 2015, Astrophys. J. , 803, 3

Kellermann K. I., Vermeulen R. C., Zensus J. A., Cohen M. H., 1998, AJ, 115, 1295

Lister M. L., et al., 2009, Astron. J. , 138, 1874

Lister M. L., Aller M. F., Aller H. D., Hodge M. A., Homan D. C., Kovalev Y. Y., Pushkarev A. B., Savolainen T., 2018, Astrophys. J. Suppl. Ser. , 234, 12

Vermeulen R. C., Ogle P. M., Tran H. D., Browne I. W. A., Cohen M. H., Readhead A. C. S., Taylor G. B., Goodrich R. W., 1995, Astrophys. J. Lett. , 452, L5